A FINITE VOLUME FORMAT FOR STRUCTURAL MECHANICS

E.Oñate

M. Cervera

E.T.S. Ingenieros de Caminos Canales y Puertos

Universidad Politécnica de Cataluña, 08034 Barcelona, Spain

and

O.C. Zienkiewicz

International Center for Numerical Methods in Engineering

Univ. Politécnica de Cataluña, 08034 Barcelona, Spain

SUMMARY

A general finite volume method (FVM) for the analysis of structural problems is presented. It is shown that the FVM can be considered to be a particular case of finite elements with a non Galerkin weighting. For structural analysis this can be readily interpreted as equivalent to the unit displacement method which involves mainly surface integrals. Both displacement and mixed FV formulations are presented for static and dynamic problems.

INTRODUCTION

The finite volume method (FVM) evolved in the early seventies via finite difference approximations on non-orthogonal grids. Popularity of the FVM has been extensive in the field of computational fluid dynamics (CFD) and heat transfer [1–5]. On the contrary, in the fied on computational solid mechanics (CSM) the use of the FVM has never achieved such acceptance. An early attempt to use FV concepts in CSM is due to Wilkins [6] as an alternative approximation to derivatives in a cell. In this he defines the average gradient of an arbitrary function u in a volume Ω as

$$\left(\frac{\partial u}{\partial x_i}\right)_\Omega \equiv \frac{1}{\Omega}\int_\Omega \frac{\partial u}{\partial x_i}\,d\Omega = \frac{1}{\Omega}\oint_S u n_i ds \tag{1}$$

using the well known divergence theorem.

Such definition of gradients can be written entirely in terms of function values at the boundary of a volume and has been used in the early "hydrocodes" of the Lawrence Livermore Laboratory.

The reasons for the unpopularity of the FVM amongst structural mechanics is understable, as finite volumes are well known to be less accurate than finite elements for self adjoint (elliptic) problems. A comparison between FVM and FEM has been recently presented by Zienkiewicz and Oñate [7]. Here the authors show that FVM and FEM share concepts such as mesh discretization and interpolation, giving precisely the same discretized systems of equations for some particular cases. Moreover, it is also shown in a simple bar example that the finite volume solution can be improved if a mixed formulation, involving displacements and stresses as variables, is used. These advantages unfortunately do not show so clearly for 2D and 3D problems. Here, surface integrals are mostly involved and the number of computations can be shown to be proportional to the number of "sides" in the mesh. This leads to an overall solution cost very similar (and sometimes greater) than that of FE computations (note that for a fine mesh of 3 node triangles the number of sides is 1.5 times that of elements). This fact suggests that computational speed is not one of the keys to the possible success of FVM in structural problems. However, the possibility of obtaining the element matrices and vectors in terms of computations along the element sides opens new possibilities for the solution of some structural problems which, in the authors' opinion, may be worth exploring in more detail.

The layout of the paper is as follows. In next section the general finite volume format for structural mechanics is presented. Both displacement and mixed formulations are discussed in detail and applications to simple bar and Timoshenko beam examples are presented. Finally, possibilities of the FVM for transient dynamic structural problems are discussed and some examples showing the potential of the methods proposed are given.

BASIC EQUATIONS

We consider the solution of the differential equations of structural mechanics and their boundary conditions which can be written as

Equilibrium equation

$$\mathbf{L}^T\boldsymbol{\sigma} + \mathbf{b}_0 - \rho\ddot{\mathbf{u}} = \mathbf{0} \quad \text{in} \quad \Omega \tag{2}$$

Strain definition

$$\boldsymbol{\varepsilon} - \mathbf{L}\mathbf{u} = \mathbf{0} \qquad \text{in} \qquad \Omega \tag{3}$$

Constitutive equation

$$\boldsymbol{\sigma} - \mathbf{D}\boldsymbol{\varepsilon} = \mathbf{0} \quad \text{in} \quad \Omega \tag{4}$$

Boundary conditions

$$\mathbf{u} - \mathbf{u}_p = \mathbf{0} \qquad \text{in} \qquad \Gamma_u \tag{5}$$

$$\mathbf{T}\boldsymbol{\sigma} - \mathbf{t}_p = \mathbf{0} \qquad \text{in} \qquad \Gamma_t \tag{6}$$

In (2)–(6) $\mathbf{u}$, $\boldsymbol{\varepsilon}$ and $\boldsymbol{\sigma}$ are the displacement, stress and strain vectors, respectively, $\mathbf{D}$ is the constitutive matrix, ρ the material density, $\ddot{\mathbf{u}}$ the vector of accelerations, $\mathbf{b}_0$ the constant body forces, $\mathbf{u}_p$ the prescribed displacements at the boundary Γ_u, $\mathbf{t}_p$ the prescribed traction forces at the boundary Γ_t, Ω the domain area or volume with boundary $\Gamma = \Gamma_u \cup \Gamma_t$. Typical examples of matrices $\mathbf{L}$ and $\mathbf{T}$ for 2D elasticity problems are

$$\mathbf{L} = \begin{bmatrix} \frac{\partial}{\partial x} & 0 \\ 0 & \frac{\partial}{\partial y} \\ \frac{\partial}{\partial y} & \frac{\partial}{\partial x} \end{bmatrix} \quad ; \quad \mathbf{T} = \begin{bmatrix} n_x & 0 & n_y \\ 0 & n_y & n_x \end{bmatrix} \tag{7}$$

where n_x, n_y are the components of the unit normal $\mathbf{n}$ to the domain boundary.

Displacement formulation

We will consider first the reduced form of eqs.(2)–(6) obtained by substituting the strains from (3) in (4) and the resulting value of the stresses in (2) and (6) to give

Equilibrium equation

$$\mathbf{L}^T\mathbf{D}\mathbf{L}\mathbf{u} + \mathbf{b}_0 - \rho\ddot{\mathbf{u}} = \mathbf{0} \quad \text{in} \quad \Omega \tag{8}$$

Boundary conditions

$$\mathbf{u} - \mathbf{u}_p = \mathbf{0} \qquad \text{in} \qquad \Gamma_u \tag{9}$$

$$\mathbf{T}\mathbf{D}\mathbf{L}\mathbf{u} - \mathbf{t}_p = \mathbf{0} \qquad \text{in} \qquad \Gamma_t \tag{10}$$

The weighted residual form of eqs.(8–10) can be written now as

$$\begin{aligned} &\int_\Omega \mathbf{W}^T[\mathbf{L}^T\mathbf{D}\mathbf{L}\mathbf{u} + \mathbf{b}_0 - \rho\ddot{\mathbf{u}}]\, d\Omega + \oint_{\Gamma_u} \mathbf{W}_u^T[\mathbf{u} - \mathbf{u}_p]\, d\Gamma + \\ &+ \oint_{\Gamma_t} \mathbf{W}_t^T[\mathbf{T}\,\mathbf{D}\,\mathbf{L}\,\mathbf{u} - \mathbf{t}_p]\, d\Gamma = \mathbf{0} \end{aligned} \tag{11}$$

We will assume now that $\mathbf{W}_u = 0$ in Γ_u enforcing the satisfaction of the kinematic boundary conditions (9). Integration by parts of the first term of the first integral in (11) and choosing $\mathbf{W}_t = -\mathbf{W}$ yields the well known expression

$$-\int_{\Omega}[\mathbf{LW}]^T\mathbf{DLu}\,d\Omega+\int_{\Omega}\mathbf{W}^T[\mathbf{b}_0-\rho\ddot{\mathbf{u}}]\,d\Omega+\oint_{\Gamma_u}\mathbf{W}^T\mathbf{TDLu}\,d\Gamma+ \\ +\oint_{\Gamma_t}\mathbf{W}^T\mathbf{t}_p\,d\Gamma=\mathbf{0} \tag{12}$$

REMARK 1

By choosing now (for 2D problems) $\mathbf{W}^T=\{\delta u,\delta v\}$, where $\delta u,\delta v$ can be intepreted as virtual displacements, eq.(12) recovers the usual form of the Principle of Virtual Displacements [8] which can be taken as the starting point for any finite element, or finite volume, formulation.

In *both* FV and FE procedures the independent unknowns are approximated as

$$\mathbf{u}\simeq\hat{\mathbf{u}}=\mathbf{N}_j\bar{\mathbf{u}}_j\qquad(j=1,\cdots,n) \tag{13}$$

where $\bar{\mathbf{u}}_j$ are the unknown parameters and $\mathbf{N}_j$ are the basis functions [8].

The approximating system of equations (12) is written now as a set of algebraic equations

$$-\int_{\Omega}[\mathbf{LW}_i]^T\mathbf{DL}\hat{\mathbf{u}}\,d\Omega+\int_{\Omega}\mathbf{W}_i^T[\mathbf{b}_0-\rho\ddot{\hat{\mathbf{u}}}]\,d\Omega+\oint_{\Gamma_u}\mathbf{W}_i^T\mathbf{TDL}\hat{\mathbf{u}}\,d\Gamma+ \\ +\oint_{\Gamma_t}\mathbf{W}_i^T\mathbf{t}_p\,d\Gamma=\mathbf{0} \tag{14}$$

where $\mathbf{W}_i\quad(i=1,\cdots,n)$ are now an appropriately selected set of weighting functions.

Eq.(14) can be written for linear systems after substitution of the interpolation (13) as

$$\mathbf{M}\ddot{\bar{\mathbf{u}}}+\mathbf{K}\bar{\mathbf{u}}=\mathbf{f} \tag{15}$$

where the usual additive property of element or subdomain contributions is preserved, whatever the form of the weighting functions. In (15) $\mathbf{M}$, $\mathbf{K}$ and $\mathbf{f}$ are, respectively, the mass and stiffness matrices and the equivalent nodal force vector given by

$$\mathbf{M}_{ij}=\int_{\Omega_i}\mathbf{W}_i\rho\mathbf{N}_j\,d\Omega \tag{16a}$$

$$\mathbf{K}_{ij}=\int_{\Omega_i}[\mathbf{LW}_i]^T\mathbf{DLN}_j\,d\Omega-\oint_{\Gamma_i}\mathbf{W}_i^T\mathbf{TDLN}_j\,d\Gamma \tag{16b}$$

$$\mathbf{f}_i=\int_{\Omega_i}\mathbf{W}_i^T\mathbf{b}_0\,d\Omega+\oint_{\Gamma_{ti}}\mathbf{W}_i^T\mathbf{t}_p\,d\Gamma \tag{16c}$$

In above Ω_i is the *control volume* associated with node i (to use the finite volume terminology. See Figure 1) where $\mathbf{W}_i \neq \mathbf{0}$. The boundary of the control volume is denoted Γ_i, excluding the part which may coincide with the external boundary of the total domain where tractions are prescribed; this particular part of the boundary is denoted as Γ_{ti} and it is included in the force term. Providing both $\mathbf{W}_i$ and $\mathbf{N}_j$ are chosen so that integrals (16) can be evaluated, then whatever the external boundary we can specify on it either the tractions ($\mathbf{t}_p$) or the displacements ($\hat{\mathbf{u}} = \mathbf{u}_p$) with equal ease.

Galerkin approach

Structural problems are usually self adjoint and the optimal weighting is the Galerkin one with $\mathbf{W}_i = \mathbf{N}_i$, thus implying the same approximation for the virtual displacements than for the actual ones. This leads to minimum energy norm errors and preserves symmetry of matrices $\mathbf{K}$ and $\mathbf{M}$ (note that the surface integral in (16b) now vanishes as N_i is zero at the control volume boundary. See Figure 2). Hence, the Galerkin approach is the basis of most frequently used finite element procedures. However, other weightings can be used recovering all possible approximation methods [8]. In what follows we shall use standard finite element interpolations $\mathbf{N}_j$ with $\bar{\mathbf{u}}_j$ standing for nodal values in element subdomains.

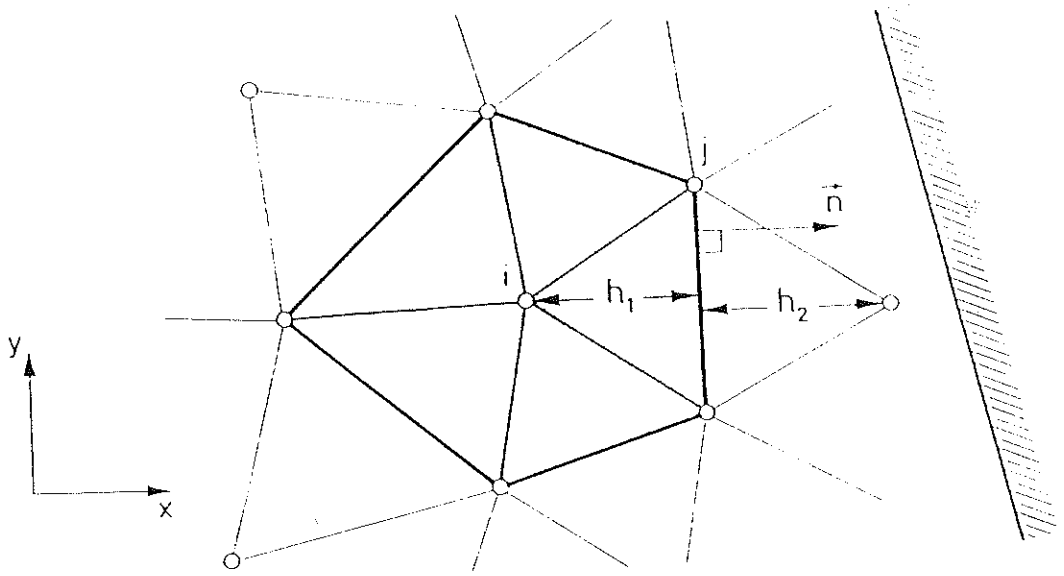

Figure 1. An assembly of finite elements/finite volumes with shading indicating the control volume.

FINITE VOLUME METHOD

The finite volume procedure is in fact a special case of the weighted eq.(14) in which

$$\mathbf{W}_i = \mathbf{I} \quad \text{in} \quad \Omega_i \quad (\text{and } \mathbf{W}_i = 0 \text{ elsewhere}) \tag{17}$$

where $\mathbf{I}$ is the unity matrix.

Eq.(14) can be readily interpreted as applying *unit virtual displacements* over each control volume. Thus substituting (17) in (12) yields (as $\mathbf{LI} = \mathbf{0}$)

$$\int_{\Omega_i} \rho\, \ddot{\hat{\mathbf{u}}} d\Omega - \oint_{\Gamma_i} \mathbf{TDL}\hat{\mathbf{u}}\, d\Gamma - \int_{\Omega_i} \mathbf{b}_0\, d\Omega - \oint_{\Gamma_{ti}} \mathbf{t}_p\, d\Gamma = \mathbf{0} \tag{18}$$

Eq.(18) can be written in the standard matrix form (15) using (13) where now

$$\mathbf{M}_{ij} = \int_{\Omega_i} \rho \mathbf{N}_j\, d\Omega \tag{19a}$$

$$\mathbf{K}_{ij} = -\oint_{\Gamma_i} \mathbf{TDLN}_j\, d\Gamma \tag{19b}$$

$$\mathbf{f}_i = \int_{\Omega_i} \mathbf{b}_0\, d\Omega + \oint_{\Gamma_{ti}} \mathbf{t}_p\, d\Gamma \tag{19c}$$

In (19) definition of Ω_i, Γ_i and Γ_{ti} coincide with those given for Equations (16). We note however that the control volume Ω_i can be prescribed in various ways, and some are discussed in the next sections.

REMARK 2

Note that in the FVM matrix $\mathbf{K}$ is invariably non–symmetric (see eqn. (19b)). This is a direct consequence of the equivalence between this approach and the well known unit displacement method in structural mechanics [12].

Cell Vertex scheme

To illustrate above concepts consider a field of arbitrary triangles with linear interpolations with the control volume for node *i-th* shown shaded in Figure 1. This corresponds in finite volume terminology to the so–called *cell vertex* approach [5] (sometimes quoted as vertex centered approach [8]).

In standard finite element assembly the weighting function $\mathbf{W}_i = \mathbf{N}_i$ is of the form shown in Figure 2a and Ω_i includes all the elements associated with the *i-th* node.

Now, if we consider the cell vertex finite volume situation (Figure 2b) it is evident that all volume integrals involving derivatives of the constant weighting function dissappear. However, a difficulty arises with the boundary

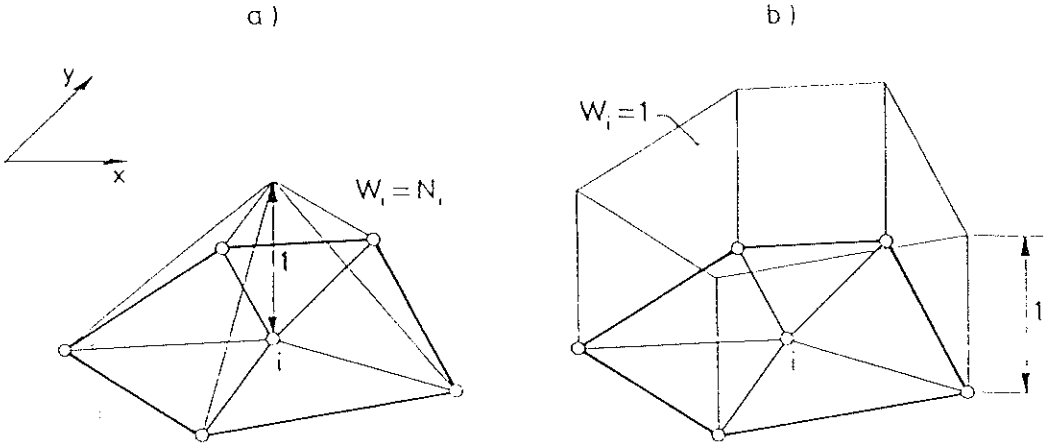

Figure 2. Weighting and basis functions for finite element (a) and finite volume (b) approximations for Figure 1.

integral in the $\mathbf{K}_{ij}$ term of Eq.(19b), because the displacement gradients involved are not continuous at the interfaces between the elements.

In the normal direction n between two elements, as illustrated in Figure 1, we have a discontinuity shown in Figure 3 with $\frac{\partial N_i}{\partial n}$ jumping from a value $1/h_1$ to $-1/h_2$, where heights of adjacent triangles are denoted h_1 and h_2.

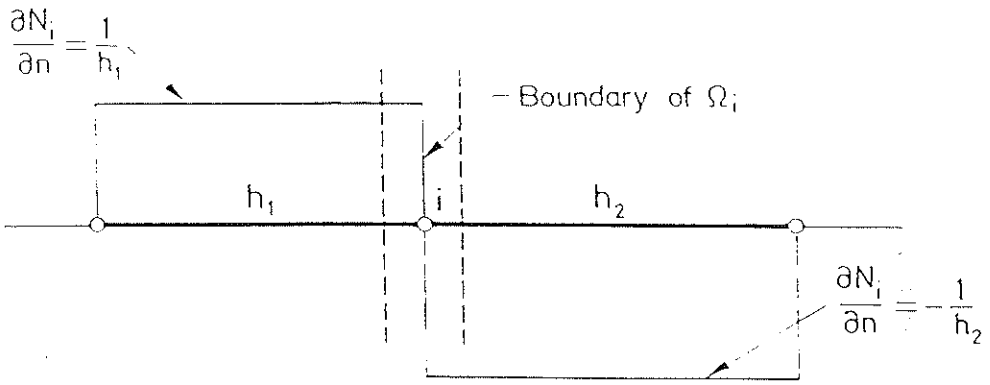

Figure 3. Discontinuity of gradient at boundaries of control volume

The theory of distributions indicates that the jump in $\frac{\partial \hat{u}}{\partial n}$ across the boundary should be given an average value. It will indeed be found that the mid value is optimal and then

$$\frac{\partial \hat{u}}{\partial n} = \frac{1}{2}\left(\left.\frac{\partial \hat{u}}{\partial n}\right|_1 + \left.\frac{\partial \hat{u}}{\partial n}\right|_2 \right) \tag{20}$$

where $\frac{\partial \hat{u}}{\partial n}|_1$ and $\frac{\partial \hat{u}}{\partial n}|_2$ are respectively the values of $\frac{\partial \hat{u}}{\partial n}$ over elements 1 and 2 sharing the interface under consideration.

REMARK 3

The jump in $\frac{\partial \hat{u}}{\partial n}$ across the boundaries reflects the discontinuity of tractions along a common boundary in two adjacent elements. This is shown clearly if the first boundary integral in (18) is written as $\oint_{\Gamma_i} \mathbf{t}\, d\Gamma$ where $\mathbf{t}$ are the tractions acting on the boundary Γ_i.

Example

An illustration of both finite element and finite volume approximations can be easily obtained in the one dimensional example of a bar under uniformly distributed traction forces, $b(x)$, where equal two node linear elements of size h are used (see Figure 4).

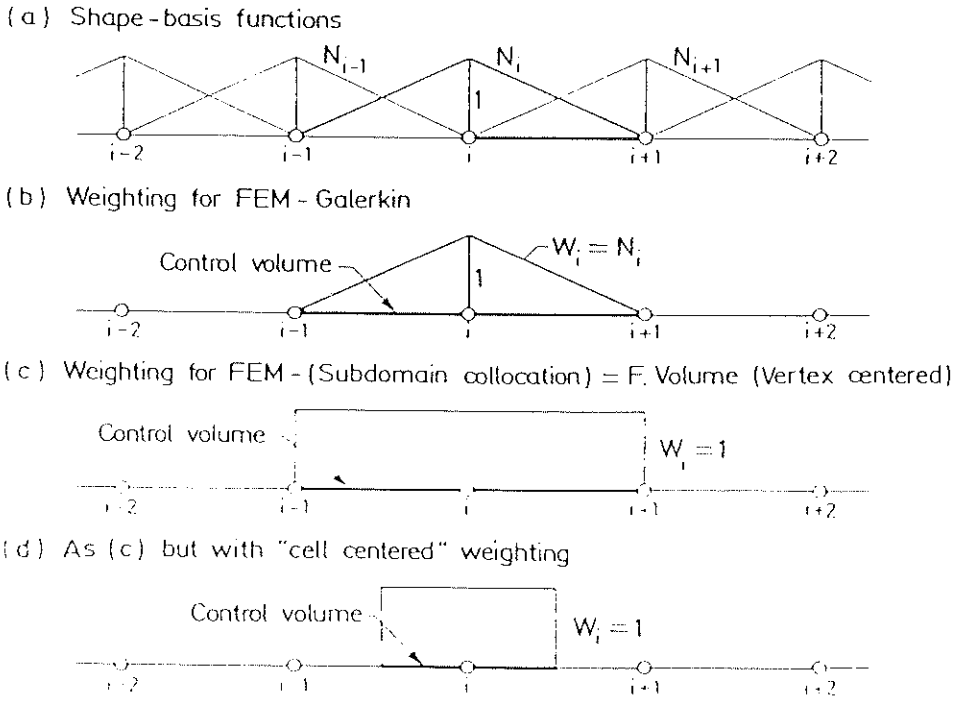

Figure 4. A one dimensional problem.

The finite element approximation yields a typical assembled equation (which can be easily verified after addition of appropriate integrals) as

$$\frac{h}{6}(\ddot{\bar{u}}_{i+1} + 4\ddot{\bar{u}}_i + \ddot{\bar{u}}_{i-1}) - \frac{k}{h}(\bar{u}_{i+1} - 2\bar{u}_i + \bar{u}_{i-1}) = f_i \tag{21}$$

where

$$f_i = \int_{-h}^{h} N_i b\, dx \tag{22}$$

The corresponding cell vertex finite volume equation is obtained using the approximation (19)–(20) as

$$\frac{h}{2}(\ddot{\bar{u}}_{i+1} + 2\ddot{\bar{u}}_i + \ddot{\bar{u}}_{i-1}) - \frac{k}{2h}(\bar{u}_{i+2} - 2\bar{u}_i + \bar{u}_{i-2}) = \bar{f}_i \tag{23}$$

where

$$\bar{f}_i = \int_{-h}^{h} b\, dx \tag{24}$$

It can be noted that the two approximations are similar but by no means identical. The finite volume considered has doubled the mass contained in the finite element. The force f_i is also doubled in case of a *constant* uniformly distributed traction b. Further the mass is not distributed in the same proportion at the nodes and neither is the force when $b = b(x)$. Also, in the FVM the stiffness term is readily recognized as an approximation to *twice* the second derivative of u. This results from using the interface derivatives given by Eq.(20). It is notorious that this stiffness term has a wider bandwith than the one corresponding to the FEM, as it involves external nodes $i-2$ and $i+2$. This is an undesiderable feature that would also occur in 2D and 3D situations, as can be seen in Figure 5. The problem can be overcome by using the so–called *cell centered* schemes, or by avoiding second order derivatives using a mixed formulation. Both possibilities are discussed in next sections.

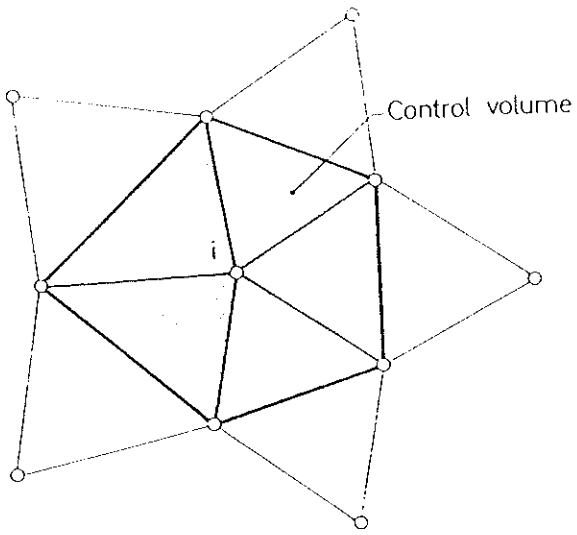

Figure 5. Nodes involved in the discretized equation of an arbitrary control volume using the cell vertex scheme and a "displacement" formulation.

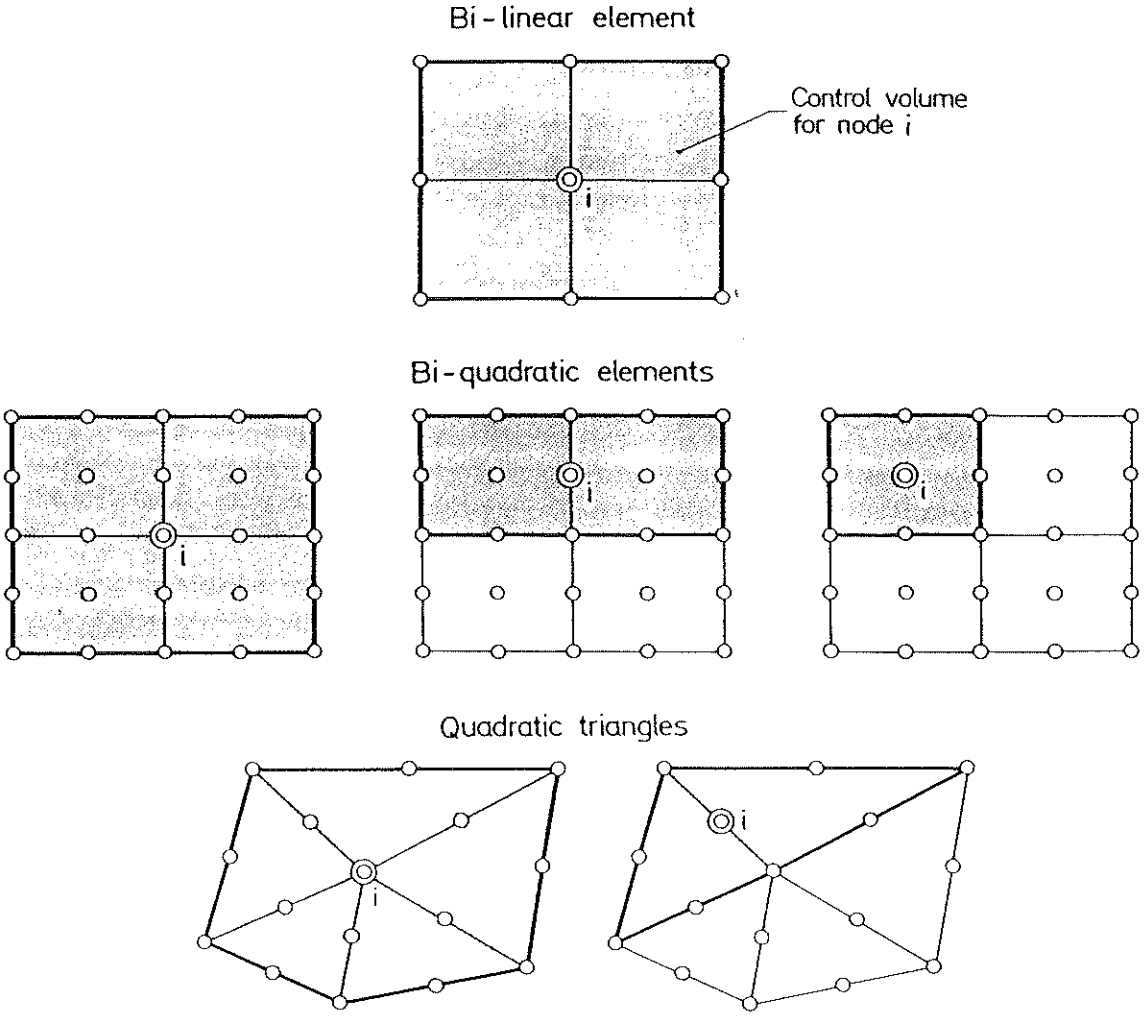

Figure 6. Control volumes for node i for higher order cell vertex schemes using quadrilateral and triangular meshes.

The cell vertex scheme can be extended to higher order interpolations without difficulty. Figure 6 shows some possibilities.

Cell centered finite volume schemes

In the preceding section we have tried to provide "weighting areas" (i.e. control volumes) coinciding with elements. Clearly this presents the difficulty of discontinuity of normal derivatives along boundaries and we can now realize why many finite volume methods are applied in so-called *cell centered* schemes. If we consider again the discretization of Figure 1 we can, as in Figure 7, assign a control volume to each node without overlapping of the

weighted area (the obvious division of each triangle is now indicated). In Figure 4 we show the one dimensional equivalent of this and the reader can easily verify that the finite volume equation now becomes

$$\frac{h}{8}(\ddot{\bar{u}}_{i+1} + 6\ddot{\bar{u}}_i + \ddot{\bar{u}}_{i-1}) - \frac{k}{h}(\bar{u}_{i+1} - 2\bar{u}_i + \bar{u}_{i-1}) = \bar{f}_i \qquad (25)$$

where

$$\bar{f}_i = \int_{-h/2}^{h/2} b\, dx$$

Equation (25) has the same connectivity as the finite element equations and indeed retrieves here exactly the stiffness terms, however showing as before different mass and force distributions.

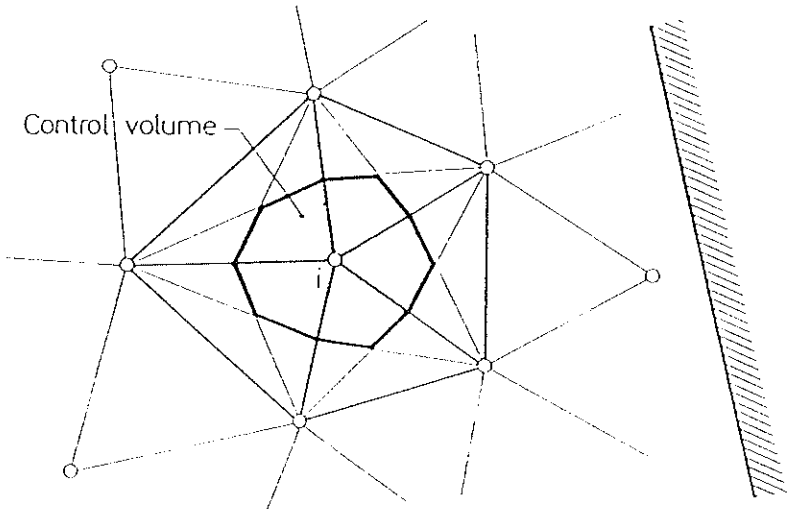

Figure 7. Cell centered control volume.

REMARK 4

The use of consistent mass forms, which is found to be beneficious in many transient computations using the finite element approximation, has never found its way into the finite volume line of thinking. Here the users invariably lump the masses implying for instance that Eq.(25) reads now

$$h\ddot{\bar{u}}_i - \frac{k}{h}(\bar{u}_{i+1} - 2\bar{u}_i + \bar{u}_{i-1}) = \bar{f}_i \qquad (26)$$

It is obvious that if lumping is used both FE and FV left-hand sides are now identical. If the forces $b(x)$ are constant, both right-hand sides are also identical, and so, the systems of equations, for the FVM and the FEM, in this particular case, are the same (and so would be for finite differences !).

For a cell centered scheme the use of mass lumping is natural, as it can be obtained integrating the corresponding terms using a nodal quadrature. This very important feature is preserved for 2D and 3D situations. Unfortunately, this is not the case for cell vertex schemes, where the mass matrices obtained are banded and not diagonally dominant.

MIXED FINITE VOLUME METHODS

The starting point for mixed methods are the equilibrium (Eq.(2)) and constitutive (Eq.(4)) equations written as

$$\mathbf{L}^T\boldsymbol{\sigma} + \mathrm{b}_0 - \rho\ddot{\mathrm{u}} = \mathbf{0} \tag{27a}$$

$$\boldsymbol{\sigma} - \mathbf{D}\mathbf{L}\mathrm{u} = \mathbf{0} \tag{27b}$$

with boundary conditions (5) and (6).

We write now the weighted residual form of Eqs.(27) and (6) as

$$\int_\Omega \mathbf{W}^T[\mathbf{L}^T\boldsymbol{\sigma} + \mathrm{b}_0 - \rho\ddot{\mathrm{u}}]\, d\Omega + \oint_{\Gamma_t} \bar{\mathbf{W}}^T[\mathbf{T}\boldsymbol{\sigma} - \mathrm{t}_p]\, d\Gamma = \mathbf{0} \tag{28a}$$

$$\int_\Omega \hat{\mathbf{W}}^T[\boldsymbol{\sigma} - \mathbf{D}\mathbf{L}\mathrm{u}] d\Omega = \mathbf{0} \tag{28b}$$

In (28a) satisfaction of the kinematic boundary conditions $\mathrm{u} = \mathrm{u}_p$ has been assumed. Integrating by parts the first term of (28a) and making $\bar{\mathbf{W}} = -\mathbf{W}$ yields

$$-\int_\Omega (\mathbf{L}\mathbf{W})\boldsymbol{\sigma}\, d\Omega + \oint_{\Gamma_u} \mathbf{W}^T\mathbf{T}\boldsymbol{\sigma}\, d\Gamma + \int_\Omega \mathbf{W}^T(\mathrm{b}_0 - \rho\ddot{\mathrm{u}})\, d\Omega + \oint_{\Gamma_t} \mathrm{t}_p\, d\Gamma = \mathbf{0} \tag{29}$$

Eqs.(29) and (28b) are the starting point for any mixed stress–displacement finite element or finite volume approximations.

We will assume now independent interpolations for the displacement and stress fields as

$$\mathrm{u} \simeq \hat{\mathrm{u}} = \mathbf{N}^u\bar{\mathrm{u}} \tag{30a}$$

$$\boldsymbol{\sigma} \simeq \hat{\boldsymbol{\sigma}} = \mathbf{N}^\sigma\bar{\boldsymbol{\sigma}} \tag{30b}$$

where $\mathbf{N}^u$ and $\mathbf{N}^\sigma$ are appropriate interpolating functions.

Choosing a cell vertex finite volume scheme with $\mathbf{W}_i = \mathbf{I}$ over each control volume, the following system of discretized equations is obtained

$$\int_{\Omega_i} \rho\,\ddot{\hat{\mathrm{u}}}\, d\Omega - \oint_{\Gamma_i} \mathbf{T}\hat{\boldsymbol{\sigma}}\, d\Gamma - \int_{\Omega_i} \mathrm{b}_0\, d\Omega - \oint_{\Gamma_{ti}} \mathrm{t}_p\, d\Gamma = \mathbf{0} \tag{31a}$$

$$\int_{\Omega_i} \hat{\mathbf{W}}_i^T[\hat{\boldsymbol{\sigma}} - \mathbf{D}\mathbf{L}\hat{\mathrm{u}}]\, d\Omega = \mathbf{0} \tag{31b}$$

where $\hat{\mathbf{W}}_i \quad (i = 1, \cdots, n)$ are appropriately selected weighting functions.

Eqs.(31) can be written in matrix form subtituting the approximations (30) as

$$\mathbf{M}\ddot{\bar{\mathbf{u}}} - \mathbf{S}\bar{\boldsymbol{\sigma}} - \mathbf{f} = \mathbf{0} \tag{32a}$$

$$\mathbf{C}\bar{\boldsymbol{\sigma}} - \mathbf{G}\bar{\mathbf{u}} = \mathbf{0} \tag{32b}$$

where

$$\begin{aligned} \mathbf{M}_{ij} &= \int_{\Omega_i} \rho \mathbf{N}_j^u \, d\Omega \quad , \qquad \mathbf{S}_{ij} = \oint_{\Gamma_i} \mathbf{T}\mathbf{N}_j^\sigma \, d\Gamma \\ \mathbf{C}_{ij} &= \int_{\Omega_i} \hat{\mathbf{W}}_i^T \mathbf{N}_j^\sigma \, d\Omega \quad , \quad \mathbf{G}_{ij} = \int_{\Omega_i} \hat{\mathbf{W}}_i^T \mathbf{D}\mathbf{L}\mathbf{N}_j^u \, d\Omega \\ \mathbf{f}_i &= \int_{\Omega_i} \mathbf{b}_0 \, d\Omega + \oint_{\Gamma_{ti}} \mathbf{t}_p \, d\Gamma \end{aligned} \tag{33}$$

Matrix $\mathbf{M}$ is in general a banded symmetric matrix, while matrix $\mathbf{C}$ is in general non–symmetric, thus rendering solution of Eq.(31a) computationally difficult. It must be noted that if a cell centered scheme and a lumping procedure are adopted, matrix $\mathbf{M}$ would become diagonal. Matrices $\mathbf{S}$ and $\mathbf{G}$ are rectangular.

Obviously, Eq.(31b) can be solved separately for each stress component. This implies solving a system of $n \times n$ equations for each stress component (n being the total number of nodes). The form of matrices $\mathbf{C}$ and $\mathbf{G}$ is obviously dependent of the choice of weighting functions $\hat{W}_i$. Here some options are possible, each one leading to a different "stress recovery" algorithm. Some of these options are discussed next.

Option 1: $\hat{\mathbf{W}}_i = \mathbf{N}_i^\sigma$ (Galerkin)

This provides symmetry of matrix $\mathbf{C}$. Furthermore, integration using a nodal quadrature would naturally produce a diagonal matrix. The resulting algorithm would be equivalent to the one suggested by Cantin et al. [9] as an improvement of standard irreductive, displacement type, finite element solutions.

Option 2 $\hat{\mathbf{W}}_i = \delta_i \mathbf{I}$ (Dirac delta)

This allows to use point collocation for direct computation of stresses as

$$\hat{\boldsymbol{\sigma}}_i = [\mathbf{D}\mathbf{L}\hat{\mathbf{u}}]_i \tag{34}$$

As the gradients are not defined at the nodes, some averaging would be needed. Obviously, this leads to the traditional nodal stress recovery method by simply averaging the stresses from the adjacent elements.

Option 3 $\hat{\mathbf{W}}_i = \mathbf{I}$

The form of matrices $\mathbf{C}$ and $\mathbf{G}$ of (33) is now given by

$$\mathbf{C}_{ij} = \int_{\Omega_i} \mathbf{N}_j^{\sigma}\, d\Omega \qquad ; \qquad \mathbf{G}_{ij} = \int_{\Omega_i} \mathbf{D}\mathbf{L}\mathbf{N}_j^{u}\, d\Omega \tag{35}$$

This would lead to nodal stress computation involving a banded $\mathbf{C}$ matrix with the same structure as matrix $\mathbf{M}$ of Eq.(33). If a cell centered scheme and mass lumping are used the resulting algorithm is equivalent to the traditional weighted nodal averaging of the stresses from the adjacent elements. This is a simple and efficient procedure.

This option can also be interpreted as equivalent to use a finite volume approach also on the constitutive equation. Integration by parts of (31b) gives

$$\begin{aligned} &\int_{\Omega_i} \hat{\mathbf{W}}_i^T [\hat{\boldsymbol{\sigma}} - \mathbf{D}\mathbf{L}^T \hat{\mathbf{u}}]\, d\Omega = \\ &= \int_{\Omega_i} \hat{\mathbf{W}}_i^T \hat{\boldsymbol{\sigma}}\, d\Omega + \int_{\Omega_i} [(\mathbf{L}^T \hat{\mathbf{W}}_i)\mathbf{D} + \hat{\mathbf{W}}_i(\mathbf{L}^T \mathbf{D})]^T \hat{\mathbf{u}}\, d\Omega - \\ &- \oint_{\Gamma_i} \hat{\mathbf{W}}_i^T \mathbf{D}\mathbf{T}^T \hat{\mathbf{u}}\, d\Gamma = \mathbf{0} \end{aligned} \tag{36}$$

Substituting now $\hat{\mathbf{W}}_i = \mathbf{I}$ in (36) yields

$$\int_{\Omega_i} \hat{\boldsymbol{\sigma}}\, d\Omega + \int_{\Omega_i} (\mathbf{L}^T \mathbf{D})^T \hat{\mathbf{u}}\, d\Omega - \oint_{\Gamma_i} \mathbf{D}\mathbf{T}^T \hat{\mathbf{u}}\, d\Gamma = \mathbf{0} \tag{37}$$

If material propierties are *constant* over the control volume the second integral of (37) vanishes and the resulting equation is

$$\int_{\Omega_i} \hat{\boldsymbol{\sigma}}\, d\Omega - \oint_{\Gamma_i} \mathbf{D}\mathbf{T}^T \hat{\mathbf{u}}\, d\Gamma = \mathbf{0} \tag{38}$$

Equation (38) relates the stresses within the control volume to the displacements in its boundary.

Transient explicit solution

Mixed finite volume methods seem particulary well suited for transient explicit problems. The staggered solution of the system (32) involves the following steps

Step 1: Displacement computation

Using central differences to discretize equation (32a) in time produces the explicit scheme

$$\bar{\mathbf{u}}^{n+1} = \Delta t^2 \mathbf{M}^{-1}[\mathbf{f}^n - \mathbf{p}_\sigma^n] + 2\bar{\mathbf{u}}^n - \bar{\mathbf{u}}^{n-1} \tag{39}$$

where $\mathbf{M}$ and $\mathbf{f}$ are given by (33), and $\mathbf{p}_\sigma$ is given by (31)

$$\mathbf{p}_{\sigma_i} = -\oint_{\Gamma_i} \mathbf{T}\hat{\boldsymbol{\sigma}}\, d\Gamma \tag{40}$$

Here use of a cell centered scheme with lumped mass matrix is most advantageous, as it only involves vector computations.

Step 2: Stress recovery

$$\bar{\boldsymbol{\sigma}}^{n+1} = \mathbf{C}^{-1}\mathbf{G}\bar{\mathbf{u}}^{n+1} \tag{41}$$

Here, the different forms of matrices $\mathbf{C}$ and $\mathbf{G}$ discussed in last section can be used. Clearly, all those resulting in a diagonal $\mathbf{C}$ matrix or leading to direct nodal averaging are computationally advantageous.

We have to note that other procedures can be used for recovery of nodal stresses. In particular the technique based on local smoothing over element patches of the Gauss point stresses obtained from the displacement values, recently proposed by Zienkiewicz and Zhu [10,11], provides superconvergent nodal stresses at a relatively low cost and could be a clearer alternative to Eq.(41).

EXAMPLE 1. AXIALLY LOADED BAR

To illustrate the applicability and performance of finite volume methods we shall consider first a simple example of an axially loaded elastic bar of lenght $2l$ (Figure 8). The axial load q will be taken either as constant (case (a) $q = c$) or linear (case (b) $q = cx$).

The equilibrium and constitutive equations and the boundary conditions read now

$$\begin{aligned} &\frac{d}{dx}\left(EA\frac{du}{dx}\right) + q = 0 && 0 \le x \le 2l \\ &u = 0 \quad \text{in} && x = 0 \\ &P = EA\frac{du}{dx} = 0 \quad \text{in} && x = 2l \end{aligned} \tag{42}$$

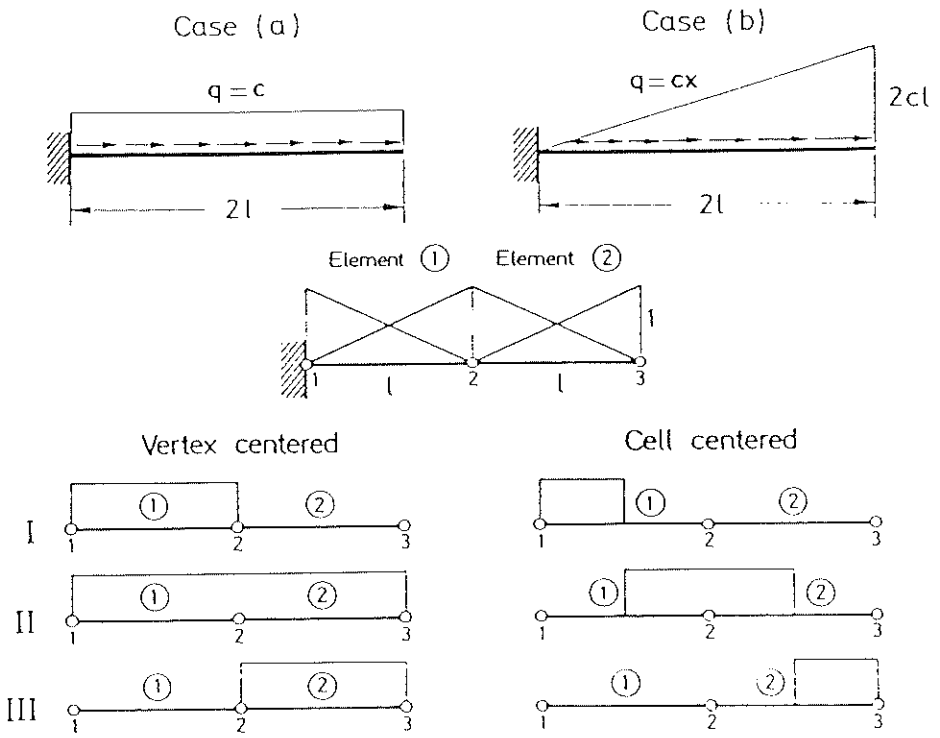

Figure 8. Elastic bar under axial load.

In above u is the axial displacement, P is the axial force and E and A are the Young modulus and the area of the bar transverse cross section respectively.

The problem will be solved with both displacement and mixed finite volume formulations using cell vertex and cell centered schemes.

Displacement FV formulation

Following the arguments of the previous sections, a typical finite volume equation can be written as

$$\left[EA\frac{du}{dx}\right]_R - \left[EA\frac{du}{dx}\right]_L + \int_{l_v} q\,dx = 0 \tag{43}$$

where L and R stand for the left and right ends of a volume of lenght l_v.

Next we discretize the bar in two node elements of equal size h. Inside each element the displacement u is linearly interpolated as

$$u = \sum_{i=1}^{2} N_i^{(e)} u_i^{(e)} \tag{44}$$

$$\text{with} \quad N_i^{(e)} = \tfrac{1}{2}(1 + \xi\xi_i) \quad \begin{cases} -1 \le \xi \le 1 \\ \xi_1 = -1, \quad \xi_2 = 1 \end{cases} \tag{45}$$

being the standard linear shape functions of the two node element.

Case (a) $q = c$ (Cell vertex and cell centered solutions)

Figure 9 shows the convergence of the cell vertex finite volume solutions for meshes of 1, 2, 3 and 4 elements, respectively.

It can be checked that, following the arguments of previous sections, the cell centered and the finite element solutions for this case are identical and *also* give the exact solution at nodes for *all* meshes.

Case (b), $q = cx$

Table I shows the percentage error of the *cell vertex* solution for the nodal axial displacements using three meshes of 1, 2 and 3 elements. Note the big error (50%) in the end displacement obtained with the one element mesh. This error reduces to 5.55% if 3 elements are used.

The *cell centered* solution differs in this case from the nodally exact finite element values due to the difference in the nodal load vectors as explained in a previous section. Percentage errors in the nodal displacements for the cell centered case are also presented in Table I and show substantial improvement with respect to the cell vertex solutions.

Mixed FV formulation

Particularization of eqs.(31) for this simple case yields (neglecting inertial terms)

$$P_R - P_L + \int_{l_v} q\, dx = 0 \tag{46a}$$

$$\int_{l_i} \hat{W} \left[P - EA \frac{du}{dx} \right] dx = 0 \tag{46b}$$

where P_R and P_L refer to axial forces values in the right and left ends of the *i-th* "finite volume" considered.

The constitutive equation will be treated following the procedure previously described as option 3; i.e. choosing $\hat{W} = 1$. Thus after integration by parts of (46b) we have

$$\int_{l_i} P\, dx - [EAu]_R + [EAu]_L = 0 \tag{47}$$

Next the bar is discretized in two node finite elements of equal size h where a linear approximation of the axial force P and the displacements u is chosen as

$$P = \sum_{i=1}^{2} N_i^{(e)} P_i^{(e)} \quad , \quad u = \sum_{i=1}^{2} N_i^{(e)} u_i^{(e)} \tag{48}$$

with $N_i^{(e)}$ given by (45).

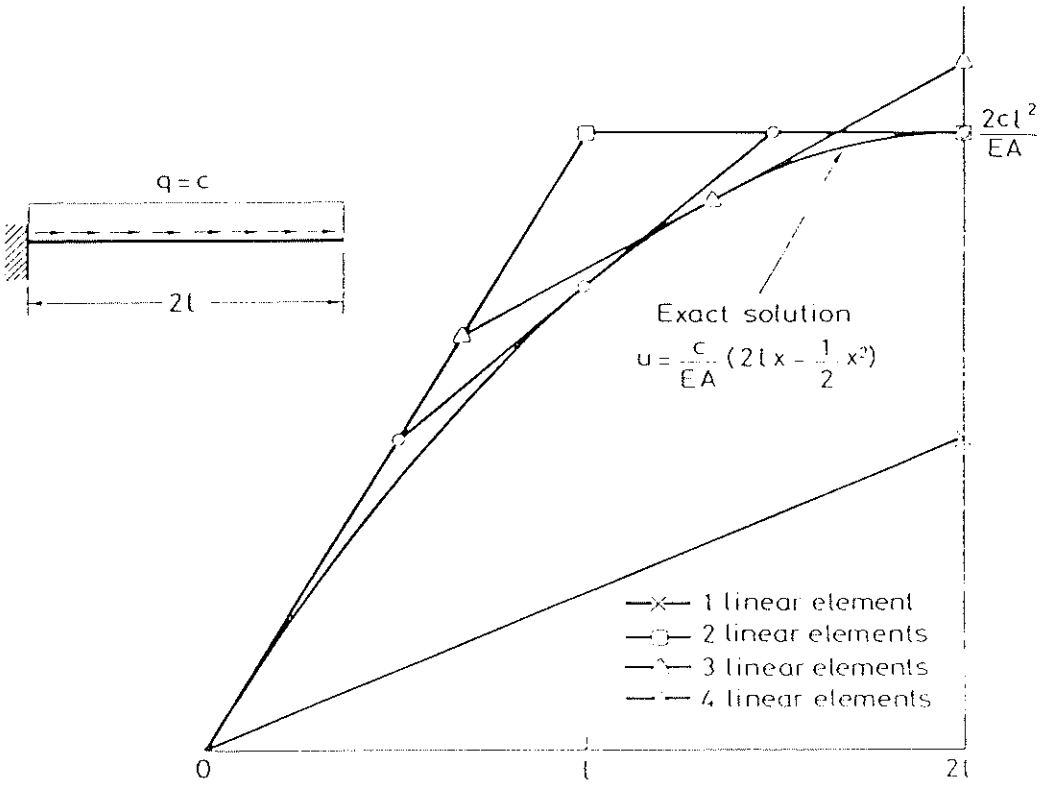

Note: The FE and FV cell centered solutions give exact nodal results in all cases.

Figure 9. Bar under constant axial load. Convergence of FV cell vertex solutions for different meshes. Displacement formulation.

Mesh	Node	FE		FV / C. Vertex		FV / C. Centered	
		Displ.	Mixed	Displ.	Mixed	Displ.	Mixed
1 el.	2	0.00%	0.00%	50.0%	25.0%	12.5%	12.5%
2 el.	2	0.00%	9.09%	9.09%	4.55%	2.27%	15.9%
	3	0.00%	0.00%	12.5%	6.66%	3.13%	3.13%
3 el.	2	0.00%	0.00%	3.85%	1.92%	0.96%	0.96%
	3	0.00%	4.35%	4.35%	2.17%	1.09%	7.61%
	4	0.00%	0.00%	5.55%	2.78%	1.39%	1.39%

Table I. Bar under linearly varying axial load. Percentage errors in nodal displacements for different meshes of linear elements using FE, cell vertex and cell centered FV schemes.

Cell Vertex solution

Substitution of (48) in (46a) and (47) yields the following system of equations for a single cell vertex domain linking nodes $i-1, i$ and $i+1$

$$P_{i+1} - P_{i-1} + f_i = 0 \qquad (49a)$$

$$\frac{h}{2}(P_{i-1} + 2P_i + P_{i+1}) + EA(u_{i-1} - u_{i+1}) = 0 \qquad (49b)$$

where $f_i = \int_{l_i} q\, dx$

Note that the boundary conditions in the end forces values must be imposed in eq.(49a) only, whereas the displacements are prescribed in eq.(49b).

It can be easily checked that results obtained for the constant load case ($q = c$) coincide precisely with the exact (displacement FE formulation) solution [7]. On the other case results for the linear load ($q = cx$) are not exact and they are shown in Table I. Note the improvement in accuracy with respect to the displacement cell vertex approach.

Cell Centered solution

Substitution of (48) in (46a) in (47) yields now the following equations for a single cell centered domain centered at node i

$$P_{i+1} - P_{i-1} + 2f_i = 0 \qquad (50a)$$

$$\frac{h}{4}(P_{i-1} + 6P_i + P_{i+1}) + EA(u_{i-1} - u_{i+1}) = 0 \qquad (50b)$$

where $f_i = \int_{l_i} q\, dx$.

The boundary conditions are treated as mentioned for the cell vertex case.

It can be easily checked that the results obtained for the constant load case ($q = c$) are very close to those obtained using a mixed FE formulation: solution, in both cases, is exact for the forces (linear field), but not for the displacements (quadratic field). Errors in displacements for the mixed FVM are slightly larger than for the mixed FEM.

Results obtained for the linear load ($q = cx$) are shown in Table I. No improvement is achieved with respect to the corresponding displacement formulation. This is probably due to the strong diagonally dominant character of eq.(50b). Note the similarities with the behaviour of the mixed FE formulation. Nevertheless, a proper rate of convergence is attained in both cases for such coarse meshes.

EXAMPLE 2. ANALYSIS OF TIMOSHENKO BEAMS

The equilibrium and constitutive equations for a Timoshenko beam are the well known equations [8]

$$\begin{aligned} &\frac{dM}{dx} + Q = 0 \\ &\frac{dQ}{dx} - q = 0 \\ &M - EI\frac{d\theta}{dx} = 0 \\ &Q - GA^*\left(\frac{dw}{dx} - \theta\right) = 0 \end{aligned} \tag{51}$$

In (51) w, θ, M and Q are the vertical displacement, the rotation of the beam sections, the bending moment and the shear force, respectively; E and G are the Young modulus and the shear modulus, I is the inertia of the cross section and $A^* = \alpha A$, where A is the beam section area and α is the shear warping coefficient ($\alpha = 5/6$ for rectangular sections).

It is well known that the displacement FE formulation for Timoshenko beam elements leads to shear locking unless reduced integration techniques are used [8]. It can be easily checked that the displacement FV approach also exhibits locking. In the FEM this deficiency can be overcome by using a mixed formulation [8]. This is also the case for the FVM, as shown below.

Mixed $w - \theta - M - Q$ FV formulation for Timoshenko beams

The weighted residual form of eqs.(51) can be written as

$$\begin{aligned} &\int_l W_1\left(\frac{dM}{dx} + Q\right)\,dx = 0 \\ &\int_l W_2\left(\frac{dQ}{dx} - q\right)\,dx = 0 \\ &\int_l W_3\left(M - EI\frac{d\theta}{dx}\right)\,dx = 0 \\ &\int_l W_4\left[Q - GA^*\left(\frac{dw}{dx} - \theta\right)\right]\,dx = 0 \end{aligned} \tag{52}$$

After adequate integration by parts of the derivative terms in (52) and choosing $W_1 = W_2 = W_3 = W_4 = 1$, the following system of equations for the *i-th* volume is obtained

$$\boxed{\begin{aligned} &M_R - M_L + \int_{l_i} Q\,dx = 0 \\ &Q_R - Q_L + \int_{l_i} b\,dx = 0 \\ &EI(\theta_L - \theta_R) + \int_{l_i} M\,dx = 0 \\ &GA^*(w_L - w_R) + \int_{l_i} GA^*\theta\,dx + \int_{l_i} Q\,dx = 0 \end{aligned}} \tag{53}$$

where again L and R denote the left and right ends of the *i-th* volume. Eqs.(53) are valid for both cell vertex and cell centered approaches. For the sake of conciseness we will consider the cell vertex solution only using linear beam elements.

Thus we will consider next a discretization of the beam of lenght l in n two node elements of equal lenght h (i.e. $nh = l$) with a linear interpolation for all displacement and stress variables. This gives the following system of discretized equations for a generic *i-th* volume formed by elements $i-1$ and i (see Figure 4)

$$M_{i+1} - M_{i-1} + \frac{h}{2}(Q_{i-1} + 2Q_i + Q_{i+1}) = 0 \tag{54a}$$

$$Q_{i+1} - Q_{i-1} + \int_{l_i} b\,dx = 0 \tag{54b}$$

$$EI(\theta_{i-1} - \theta_{i+1}) + \frac{h}{2}(M_{i-1} + 2M_i + M_{i+1}) = 0 \tag{54c}$$

$$GA^*(w_{i-1} - w_{i+1}) + \frac{GA^*h}{2}(\theta_{i-1} + 2\theta_i + \theta_{i+1}) + \frac{h}{2}(Q_{i-1} + 2Q_i + Q_{i+1}) = 0 \tag{54d}$$

Note that the boundary conditions for M, Q, θ and w must be imposed in equations (54a), (54b), (54c) and (54d), respectively.

Eqs.(54) will be now applied to the analysis of a clamped–free beam under a point load acting at the free end (see Figure 10). It can be shown that the solution using one beam element gives

$$\theta_2 = -\frac{Pl^2}{2EI}\ \text{(exact)} \qquad w_2 = -P\left[\frac{l}{GA^*} + \frac{l^3}{4EI}\right] \tag{55}$$

Solution for the end deflection coincides with that obtained with the finite element displacement approach using one point reduced integration for the shear stiffness terms [8] and differs slightly from the exact value $\left(w_2 = -P\left[\frac{l}{GA^*} + \frac{l^3}{3EI}\right]\right)$. Table II shows the convergence of the end deflection values obtained with meshes of 1,2 and 3 linear beam elements. Note that the end deflection obtained is exact for all the meshes.

EXACT	$w = -P\left[\frac{l}{GA^*} + \frac{l^3}{3EI}\right]$	$\theta = -P\frac{l^3}{2EI}$
1 element	$w = -P\left[\frac{l}{GA^*} + \frac{l^3}{4EI}\right]$	*end rotation exact*
2 elements	$w = -P\left[\frac{l}{GA^*} + \frac{l^3}{\frac{16}{5}EI}\right]$	*end rotation exact*
3 elements	$w = -P\left[\frac{l}{GA^*} + \frac{l^3}{\frac{108}{35}EI}\right]$	*end rotation exact*

Table II. End deflection values for clamped-free beam under point load acting at the free end. Mixed $w - \theta - M - Q$ cell vertex formulation.

Mixed $w - \theta - Q$ FV formulation

Substituting (51c) in (51a) yields the following system of equations

$$\begin{aligned} &\frac{d}{dx}\left(EI\frac{d\theta}{dx}\right) + Q = 0 \\ &\frac{dQ}{dx} - q = 0 \\ &Q - GA^*\left(\frac{dW}{dx} - \theta\right) = 0 \end{aligned} \tag{56}$$

Following the arguments of previous sections the following system of equations for the *i-th* volume can be obtained

$$\boxed{\begin{aligned} &EI\left(\frac{d\theta}{dx}\right)_R - EI\left(\frac{d\theta}{dx}\right)_L + \int_{l_i} Q\,dx = 0 \\ &Q_R - Q_L - \int_{l_i} b\,dx = 0 \\ &GA^*(w_L - w_R) + \int_{l_i} GA^*\theta\,dx + \int_{l_i} Q\,dx = 0 \end{aligned}} \tag{57}$$

Computation of the derivatives $\left(\frac{d\theta}{dx}\right)_R$ and $\left(\frac{d\theta}{dx}\right)_L$ can be done following the averaging procedure of eq.(20).

Application of (57) for the beam problem of Figure 10 with one linear beam elements gives

$$\theta_2 = \frac{-Pl^2}{EI} \quad , \quad w_2 = -P\left[\frac{l}{GA^*} + \frac{l^3}{2EI}\right] \tag{58}$$

Note that neither θ_2 nor w_2 are now exact. However the solutions does not lock. Convergence of the end deflection and rotation values for this case with meshes of 1,2 and 3 elements is shown in Table III.

EXACT	$w = -P\left[\frac{l}{GA^*} + \frac{l^3}{3EI}\right]$	$\theta = -P\frac{l^2}{2EI}$
1 element	$w = -P\left[\frac{l}{GA^*} + \frac{l^3}{2EI}\right]$	$\theta = -P\frac{l^2}{EI}$
2 elements	$w = -P\left[\frac{l}{GA^*} + \frac{l^3}{\frac{8}{3}EI}\right]$	$\theta = -P\frac{l^2}{2EI}$ (exact)
3 elements	$w = -P\left[\frac{l}{GA^*} + \frac{l^3}{\frac{54}{19}EI}\right]$	$\theta = -P\frac{l^2}{\frac{9}{5}EI}$

Table III. End deflection values for clamped-free beam under point load acting at the free end. Mixed $w - \theta - Q$ cell vertex formulation.

EXAMPLE 3. TRANSIENT 2D ELASTICITY

To illustrate the applicability and performance of FV methods in the context of transient 2D elasticity we shall consider a simple example of an elastic bar of dimensions 10x1x1 under plane stress conditions (Figure 10). The material properties selected are: Young modulus $E = 1.0x10^{-2}$, Poisson's ratio $\nu = 0.1$, and density $\rho = 1.0$. Two load cases will be considered: (a) body forces $\mathbf{b}_0$ constant acting in the direction of the bar, and (b) body forces $\mathbf{b}_0$ contant acting in the direction normal to the bar. Case (a) would be really a one–dimensional stress wave propagation problem if Poisson's effect was neglected. Case (b) is a free oscillation problem under lateral load.

The problem will be solved with both displacement and mixed finite volume formulations using cell centered schemes, which provides naturally a lumped mass matrix.

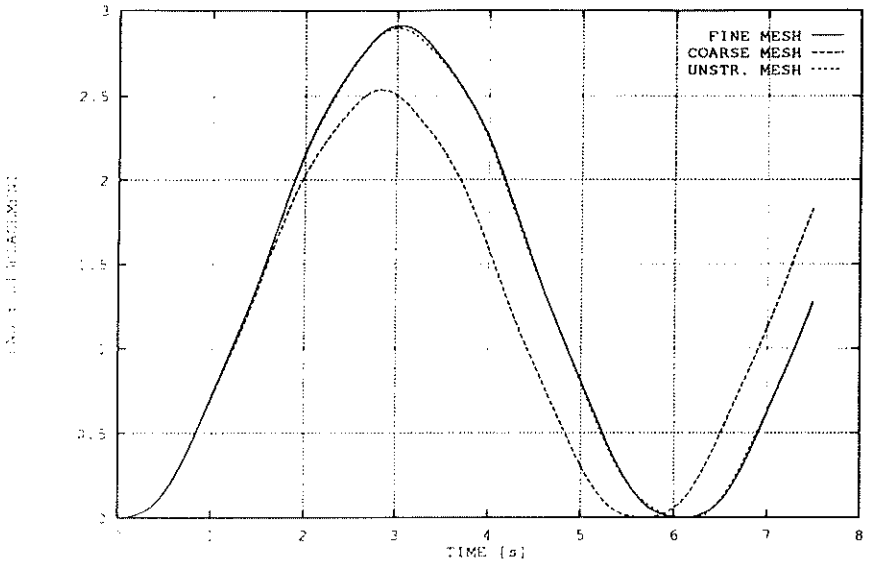

Figure 12 Example 3(b). Deflection at the end of the bar with the displacement formulation. FV and FE results coincide.

where the term involving prescribed tractions has been omitted again for simplicity. Note that the constitutive equation (61b) has been treated following the procedure described as option 3, i.e. choosing $\hat{W} = 1$. As remarked in a previous section, this option, combined with a cell centerd scheme with lumped C matrix, is equivalent to a weighted nodal averaging of stresses from the adjacent elements.

We discretize the bar in three node elements. Inside each element the displacements u and the stresses $\boldsymbol{\sigma}$ are linearly interpolated as

$$\mathbf{u} = \sum_{i=1}^{3} \mathbf{N}_i^u \mathbf{u}_i \quad , \quad \boldsymbol{\sigma} = \sum_{i=1}^{3} \mathbf{N}_i^\sigma \boldsymbol{\sigma}_i \tag{62}$$

being N_i^u and N_i^σ the standard linear shape functions of the three node element.

Case (a): body forces in the direction of the bar

The results obtained for the end deflection using mesh (1) with both FV and FE (with lumped mass) methods overlap with those plotted in Figure 11. It can be proved that also for the mixed formulation FV and FE results are approximately the same for constant body loads, and in fact they coincide exactly if an additional approximation is admitted when performing the appropriate boundary integrals in the FVM (see eq.(A.8) in Appendix).

Case (b): body forces normal to the bar

Figure 13 shows the end deflection of the bar using meshes (1), (2) and (3), and the FV method, with linear interpolation for both displacements and stresses. It has to be pointed out again that these results are equal to those provided by the mixed FEM, as the load is constant, and the approximation described in the Appendix has been used. Remembering that the thin beam theory exact solution has a peak deflection of 3.0, it is remarkable to see that the mixed method provides a convergent solution with larger displacements than the exact solution. The results show again how the unstructured mesh achieves almost the same accuracy as the fine regular mesh with one third of the CPU cost.

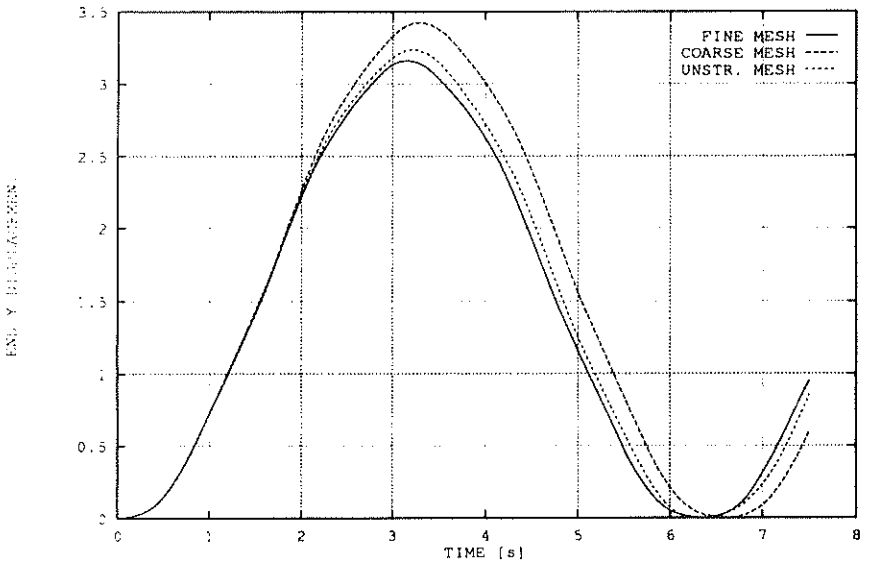

Figure 13. Example 3(b). Deflection at the end of the bar with the FVM mixed formulation. FV and FE results coincide.

FORMULATION	TOTAL CPU time (s)	INT. FORCES EVAL. CPU time (s)	STRESS EVAL. CPU time (s)
Displ.–FEM	474.39	242.87	133.57
Displ.–FVM	508.75	277.12	134.13
Mixed–FEM	763.91	294.88	370.39
Mixed–FVM	880.19	412.42	363.70

Table IV. CPU time comparison between the different formulations for case (b). Fine mesh

Finally, Table IV shows the comparison between the CPU times spent for the solution of problem 3b using the different formulations, for the fine mesh. The problem has been run in a CONVEX C-120 machine (one vectorial processor). It can be seen that the displacement formulations are far less costly than the mixed ones, due to the fact that they only require solution of one set of equations. CPU time comparison between FEM and FVM is favorable to the first, but only slightly for the irreductible case.

CONCLUSIONS

The Finite Volume Method (FVM) is presented in a format applicable to structural mechanics. It is shown that the FVM can be considered as a particular case of Finite Elements with a non–Galerkin weighting, equivalent to the use of a constant virtual displacement field. The resulting equations are identical to those provided by the well known unit displacement method.

The displacement FVM is discussed and both cell vertex and cell centered schemes have been examined. Cell centered schemes are preferable because they provide naturally diagonal mass matrices, and the internal force terms as the FEM. Thus, for constant body forces the FE and FV solutions are identical.

The mixed FVM has been also discussed, with different options for the weighting of the constitutive equation. Again, cell centered schemes are preferable because they provide naturally diagonal matrices for both equations. It is shown that weighted nodal averaging of stresses is a simple and valid alternative. Explicit transient analysis is presented in this context, both by its intrinsic interest, and as an iterative procedure to solve static problems.

Example 1 proves that the cell centered scheme is more accurate than the cell vertex scheme for the simple problem presented. Also, the benefits of a mixed formulation are underlined.

Example 2 shows the possibilities of mixed FVM for bending problems, as the two schemes proposed are convergent and present no locking, as expected.

Example 3 shows the possibilities of displacement and mixed FVM in plane elasticity. It is demostrated that under constant loads, FV and FE approximations produce *exactly* the same systems of equations, and thus, the same results, for the irreductible formulation. This is also the case for the mixed formulation if an additional approximation is admitted when performing the appropiate boundary integrals.

It seems that the merits of the FVM could lay in the possibility of computing element matrices and vectors using boundary integrals along the control volume sides, involving information provided by adjacent elements. This feature is currently under investigation by the authors.

ACKNOWLEDGMENT

The authors wish to express their gratitude to Mr. R. Codina for his useful comments during the realization of this work.

REFERENCES

[1] MacDonald, P.W. "The computation of transonic flow through two dimensional gas turbine cascades", *ASME* paper 71-GT-89, 1971.

[2] MacCormack, R.W. and Paullay, A.J. "Computational Efficiency achieved by time splitting of finite difference operators", *AIAA*, 72–154, San Diego, 1972.

[3] Rizzi, A.W. and Inouye, M. "Time split finite volume method for three dimensional blunt-body flows", *AIAA Journal*, 11, 1478–85, 1973.

[4] Patankar, S.V., "*Numerical heat transfer and fluid flow*", Series in Computational Methods in Mechanics and Thermal Sciences, W.J. Minkowycz and E. M. Sparrow (Eds.), Hemisphere Publising Corp., 1980.

[5] Hirsch, C. "*Numerical computation of internal and external flow*", Vol. I, J. Wiley, 1989.

[6] Wilkins, M.L. "Calculations of elasto-plastic flow". *Methods of Computational Physics* (Eds. Balder et al.), Vol. 3, Academic Press, 1964.

[7] Zienkiewicz, O.C. and Oñate, E. "Finite elements versus finite volumes. Is there really a choice ?", in *Nonlinear Computation Mechanics. State of the Art.* P. Wriggers and W. Wagner. Springer–Verlag, 1991.

[8] Zienkiewicz, O.C. and Taylor, R.L. *The finite element method.* McGraw Hill, 1989 (Vol. I) and 1991 (Vol. II).

[9] Cantin, G., Loubignac, G. and Touzot, G. "An iterative algorithm to build continuous stress and displacement solutions", *Int. J. Num. Meth. Eng.*, Vol. 12, 1493–1506, 1978.

[10] Zienkiewicz, O.C. and Zhu, J.Z. "Superconvergent derivative recovery techniques and a posteriori error estimations in the finite element method. Part I: A general superconvergent recovery technique", Internal Report CR/671/91, Univ. Coll. of Swansea, 1991. To be published in *Int. J. Num. Meth. Eng.*.

[11] Zienkiewicz, O.C. and Zhu, J.Z. "Superconvergent derivative recovery techniques and a posteriori error estimations in the finite element method. Part I: The Zienkiewicz–Zhu a posterior error estimator", Internal Report CR/672/91, Univ. Coll. of Swansea, 1991. To be published in *Int. J. Num. Meth. Eng.*.

[12] Gallagher, R.H. "A correlation study of matrix structural analysis". AGAR Dograph 69, Pergamon Press, 1964.

APPENDIX

It was stated in Example 3 that both FV (cell centered scheme) and FE approximations produce the same internal force terms for the displacement and mixed formulations, when 3 noded linear elements are used. That is to say that the vectors

$$\mathbf{p}_\sigma^{FE} = \int_{\Omega_i} (\mathbf{L}\,\mathbf{N})^T \boldsymbol{\sigma}\, d\Omega \qquad (A.1a)$$

$$\mathbf{p}_\sigma^{FV} = -\oint_{\Gamma_i} \mathbf{T}\,\boldsymbol{\sigma}\, d\Gamma \qquad (A.1b)$$

are identical component by component.

Let us consider first the *displacement formulation*. The *k-th* component of the *i-th* node of the internal force vector for FE is, from (A.1a), and using tensor notation for the stresses,

$$\begin{aligned} p_{ik}^{FE} &= \int_{\Omega_i} \frac{\partial N_i}{\partial x_j}\sigma_{jk}\, d\Omega = \\ &= \sum_{e=1}^{n_{el}} \int_{\Omega_i^e} \frac{\partial N_i^e}{\partial x_j}\sigma_{jk}^e\, d\Omega = \\ &= \sum_{e=1}^{n_{el}} \sigma_{jk}^e \int_{\Omega_i^e} \frac{\partial N_i^e}{\partial x_j}\, d\Omega \end{aligned} \qquad (A.2)$$

for a patch of n_{el} elements concurrent at node i (Figure A.1).

On the other hand, the *k-th* component of the *i-th* node of the internal force vector for FV is from (A.1b)

$$\begin{aligned} p_{ik}^{FV} &= -\oint_{\Gamma_i} n_j\sigma_{jk}\, d\Gamma = \\ &= \sum_{e=1}^{n_{el}} -\int_{\Gamma_i^e} n_j\sigma_{jk}^e\, d\Gamma = \\ &= \sum_{e=1}^{n_{el}} \sigma_{jk}^e \left(-\int_{\Gamma_i^e} n_j\, d\Gamma\right) \end{aligned} \qquad (A.3)$$

But, for the *e-th* element, with sides of lenght l_1, l_2, l_3 and external unit normals $\mathbf{n}_1$, $\mathbf{n}_2$, and $\mathbf{n}_3$, respectively (see Figure A.1), we can write

$$\begin{aligned}\int_{\Omega_i^e} \frac{\partial N_i^e}{\partial x_j}\, d\Omega &= \int_{\partial\Omega_i^e} n_j N_i^e\, d\Gamma = \\ &= n_{1j}\frac{1}{2}l_1 + n_{2j}\frac{1}{2}l_2 = \\ &= -n_{3j}\frac{1}{2}l_3 = \\ &= -\int_{\Gamma_i^e} n_j\, d\Gamma\end{aligned} \tag{A.4}$$

where $\partial\Omega_i^e$ is the complete boundary of element e, while Γ_i^e is the part of the boundary of the cell Ω_i *interior* to element e.

With the result from (A.4) the identity $p_{ik}^{FE} = p_{ik}^{FV}$ is demonstrated.

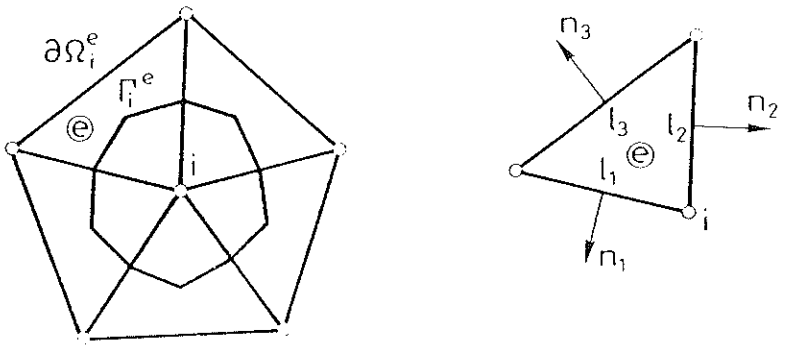

Figure A.1 A patch of elements concurrent at node i-th

Let us consider now the *mixed formulation* with linear interpolations for both displacements and stresses:

The *k-th* component of the *i-th* node of the internal force vector for FE is from (A.1b)

$$\begin{aligned}p_{ik}^{FE} &= \int_{\Omega_i} \frac{\partial N_i}{\partial x_j}\sigma_{jk}\, d\Omega = \\ &= \sum_{e=1}^{n_{el}} \int_{\Omega_i^e} \frac{\partial N_i^e}{\partial x_j}\sigma_{jk}^e\, d\Omega = \\ &= \sum_{e=1}^{n_{el}} \int_{\Omega_i^e} \frac{\partial N_i^e}{\partial x_j}\left(\sum_{r=1}^{3} N_r^e \sigma_{jk}^r\right) d\Omega\end{aligned} \tag{A.5}$$

Being the shape functions N_r linear, this integral can be evaluated using the values of σ_{jk} at the centroid of the triangle, that is

$$\bar{\sigma}_{ij}^{e} = \frac{1}{3} \sum_{r=1}^{3} \sigma_{jk}^{r} \tag{A.6}$$

and then

$$p_{ik}^{FE} = \sum_{e=1}^{n_{el}} \bar{\sigma}_{jk}^{e} \int_{\Omega_i^e} \frac{\partial N_i}{\partial x_j} \, d\Omega \tag{A.7}$$

On the other hand, the *k-th* component of the *i-th* node of the internal force vector for FV is from (A.1b)

$$\begin{aligned} p_{ik}^{FV} &= - \oint_{\Gamma_i} n_j \sigma_{jk} \, d\Gamma = \\ &= \sum_{e=1}^{n_{el}} - \int_{\Gamma_i^e} n_j \sigma_{jk}^{e} \, d\Gamma = \\ &= \sum_{e=1}^{n_{el}} - \int_{\Gamma_i^e} n_j \left(\sum_{r=1}^{3} N_r^e \sigma_{jk}^{r} \right) \, d\Gamma \\ &\simeq \sum_{r=1}^{n_{el}} \bar{\sigma}_{jk}^{e} \left(- \int_{\Gamma_i^e} n_j \, d\Gamma \right) \end{aligned} \tag{A.8}$$

Note that the last step in (A.8) is an approximation, as the stresses σ_{jk}^{e} are linear inside the element.

Comparing (A.5) with (A.8), and using the result from (A.4), the expression $p_{ik}^{FE} \simeq p_{ik}^{FV}$ is demonstrated.